Validated Model of Thermochemical Energy Storage Based on Cobalt Oxides

Xin Zhou[1], Mariam Mahmood[2, 3*], Jinli Chen[1], Tianfeng Yang[1], Gang Xiao[1*], Mario L. Ferrari[2]
[1] State Key Laboratory of Clean Energy Utilization, Zhejiang University, China
[2]Department of Mechanical Engineering (DIME), University of Genova, Italy
[3] U.S.-Pakistan Center for Advanced Studies in Energy (USPCAS-E)-National University of Sciences and Technology (NUST), Pakistan
*Email: mariam@uspcase.nust.edu.pk, mariam.mahmood@edu.unige.it
*Email: xiaogangtianmen@zju.edu.cn

Highlights:

- A dynamic model of a thermochemical storage module is presented for plant analysis.
- The 1-D model was validated with the experimental data from literature.
- Good temperature matching and error of energy amount within 20% were obtained.
- Thermochemical energy density was 16.65% higher than sensible energy density.
- Parametric analysis for optimizing a thermochemical storage module was performed.

Validated Model of Thermochemical Energy Storage Based on Cobalt Oxides

Xin Zhou[1], Mariam Mahmood[2, 3*], Jinli Chen[1], Tianfeng Yang[1], Gang Xiao[1*], Mario L. Ferrari[2]
[1] State Key Laboratory of Clean Energy Utilization, Zhejiang University, China
[2]Department of Mechanical Engineering (DIME), University of Genova, Italy
[3] U.S.-Pakistan Center for Advanced Studies in Energy (USPCAS-E)-National University of Sciences and Technology (NUST), Pakistan
*Email: mariam@uspcase.nust.edu.pk, mariam.mahmood@edu.unige.it
*Email: xiaogangtianmen@zju.edu.cn

Abstract

Thermal Energy Storage (TES) can play a critical role through provision of reliable energy supply and increase the market penetration of renewable energy sources. Thermochemical Energy Storage (TCES) based on reversible reactions offers distinguished advantages in comparison with sensible and latent heat storage: higher energy density, higher temperature range and possibility of seasonal storage. TCES systems based on the redox cycle of metallic oxides shows significant potential for integration with Concentrated Solar Power (CSP) plants using air as the heat transfer fluid, which also acts as a reactant for the redox reaction. A pilot scale thermochemical storage reactor designed for a CSP plant has been developed and tested in the framework of a collaborative European funded project "RESTRUCTURE" at the Solar Tower Julich (STJ). TCES system is proposed with the aim of achieving higher energy storage capacity and higher storage temperature. Numerical modeling of a TCES prototype presented in this study is a contribution towards this effort. The present work is focused on the innovative one-dimensional modeling of a TCES system based on the redox cycle of cobalt oxides (Co_3O_4/CoO), coated on the ceramics honeycomb structures. The numerical model for TCES involved the energy balance and reaction kinetics describing the redox reaction of cobalt oxides, to simulate the phenomena of thermochemical storage. The simulation results were presented as the temperature profiles at different positions inside the storage vessel and they were validated against experimental data published in literature by other groups. This validation proved that this model can simulate the overall thermochemical storage process with reasonable accuracy. The simulation tool was also used to perform the parametric analysis of the storage module, which provides guidance to optimize the performance of the storage system. Moreover, due to its good

compromise between reliability and computational time, the established 1-D thermochemical storage model can be integrated with the CSP plant model for dynamic analysis of the whole system, which is the aim of this study.

Keywords: Thermochemical storage; Cobalt oxides; Redox cycle; Numerical model.

1. Introduction

The restricted supply of fossil fuels and associated environmental problems have gradually become the bottleneck for world economic growth. This scenario is fostering the utilization of renewable energy sources to mitigate tension between the growing energy demand and public concerns on the environmental deterioration caused by fossil fuels [1]. The accelerated deployment of renewable energy can help the emerging economies through provision of clean and secure energy supply, and thus achieving the 'green economy' without compromising their economic growth [2].

Solar power is currently one of the most promising renewables due to its wide availability, cost effectiveness and ease of hybridization. However, the intermittent nature of solar energy makes the energy storage inevitable for dispatchable power generation and the grid integration. Concentrating Solar Power (CSP), one of the two main technologies of solar power, is featured by the ease of hybridization with large-scale and inexpensive thermal storages, which bridge the gap between energy demand and supply, thus facilitates the grid integration. This significantly increases the CSP capacity factor, thus giving it an edge over solar PV and other renewables, and making the CSP power plants economically viable [2-5].

Thermal storage can be based upon the following basic principles: Sensible Heat Storage (SHS) [6, 7] where heat is stored by increasing the storage medium temperature; latent heat storage, where energy is stored during the phase transition of Phase Change Materials (PCM); Thermochemical Energy Storage (TCES) where energy is stored in reversible chemical reactions [8]. SHS represents the simplest and least expensive form of thermal storage. However, due to low energy density (i.e. three or five times lower than that of latent and thermochemical energy storage systems, respectively), SHS requires large volumes to store sufficient amount of energy, resulting in much of the costs for installation, adjustment and maintenance [9].

PCMs such as paraffin and fatty acids provide relatively high energy density within limited temperature ranges, which are appropriate for heat storage systems with short duration [10]. However, they suffer from greatly reduced heat transfer coefficient during phase change processes, which increases the cost and technical challenges for large-scale thermal storage systems. TCES offers potential benefits, such as high energy density, possibility of long-term seasonal storage and higher temperature range. However, this technology is still under development [11].

TCES systems are based on the reversible chemical reaction: concentrated solar power drives an endothermic reaction during daytime, i.e. charging phase, and stored thermal energy is recovered during the exothermic reaction taking place during the off-sun operation, i.e. discharging phase. The heat generated during the exothermic reaction can be used for power production or heating applications. The chemical energy stored (Eq.1) in the complete cycle depends on the reaction enthalpy (ΔH_r), extent of conversion (α) and mass of the reactant (m) [12]:

$$Q = \alpha \cdot m \cdot \Delta H_r \tag{1}$$

TCES systems store sensible as well as chemical energy, thus are capable to achieve higher energy density in comparison with sensible and latent heat storage. During past few decades, several materials have been tested as potential candidates to optimize the TCES performance: carbonation/decarbonation of metal oxides/carbonates, hydration/dehydration of salt hydrates, decomposition/sulfation of metal sulfates/oxides, ammonia synthesis/dissociation and reduction/oxidation (redox) of metal oxides [13].

Important salt hydrates for TCES include $MgSO_4.7H_2O$, $MgCl_2$ / H_2O and $SrBr_2$ /H_2O. When heated to a threshold temperature, the salts hydrates dissociate into anhydrous salt and water vapor i.e. dehydration, and store thermal energy. During discharging process, water vapor flows across the anhydrous salt and hydration occurs releasing the stored energy. These salts have high volumetric heat capacity, large thermal conductivity, and are also less expensive in comparison with PCMs. However, several technical challenges such as liquid super-cooling, recrystallization and nucleation effects during hydration and lower stability make the salt hydrates inapplicable for cyclic use [14].

Balasubramanian et al. [14] have developed a mathematical model to investigate the capability of magnesium sulphate heptahydrate ($MgSO_4.7H_2O$) salt to store thermochemical energy. This model is based on the mass and energy balance and desorption kinetics which govern the dehydration process. A parametric study by this model provides guidance about the characteristics of optimal materials for thermochemical storage: salt hydrates of larger thermal conductivity, higher specific heat capacity and lower thermochemical desorption rates can improve the process performance. In the next study, the Authors have also modeled the heat release during hydration reaction. A robust sensitivity analysis helps to identify the parameters that significantly influence the heat release process such as heat capacity, heat flux and flow rate, thus can help to optimize the process efficiency [15].

Lele at al. [16] has established a mathematical model based on the set of partial differential equations (PDEs) describing the mass and energy conservation and reaction kinetics during thermal desorption of salt hydrates in a fixed bed storage reactor. The thermal behavior and desorption dynamics in the reactor based on the modified Prout-Tompkins equations are studied at room temperature (293 K) and bed pressure of 12 mbar. Overall work is aimed to develop an adaptive modelling approach and correct set of PDEs to demonstrate the thermal decomposition of salt hydrates and hence optimization of the system parameters.

The reduction/oxidation (redox) of metal oxides is the most suitable thermochemical reaction for CSP plants using air as heat transfer medium: since oxygen required for redox reaction can be supplied by the air, thus avoiding the separate gas storage. During charging, hot air from solar receiver flows through the storage reactor, where heat is transferred to the solid material to raise its temperature (i.e. sensible storage). When solid temperature achieves the equilibrium temperature of reduction, endothermic reaction takes place (i.e. chemical storage). During discharging, cold air flows through the storage reactor where first it extracts the sensible energy, and hence solid temperature decreases. When solid temperature decreases to the equilibrium temperature of oxidation, exothermic reaction takes place and chemical energy is absorbed by the air.

Metallic redox pair oxides such as Co_3O_4/CoO, BaO_2/BaO, Mn_2O_3/Mn_3O_4, CuO/Cu_2O and Fe_2O_3/Fe_3O_4 have been studied for CSP plants [17, 18]. Group of Karagiannakis et al. [19,20]

have performed relatively complete research from perfomance analysis of different redox pair materials to opitimized design of thermalchemical storage module for a 70.5 MWe CSP plant, which is in the framework of a collaborative European funded project "RESTRUCTURE" at the Solar Tower Julich (STJ). Co_3O_4/CoO redox pair (Eq.2) has the most favorable characteristics: its redox temperature is perfectly suitable for solar tower power plants (equilibrium temperature is about 900°C, at atmospheric pressure); higher energy density than other oxides (844 kJ/kg for complete conversion); good reaction kinetics and long-term material stability for redox cycling [19-22].

$$Co_3O_4 \overset{\Delta H}{\leftrightarrow} 3CoO + 1/2O_2 \qquad \Delta H_r = 196 kJ/mol \tag{2}$$

Tescari et al. [23] have carried out an experimental campaign on a pilot scale thermochemical storage reactor designed for a CSP plant 'Solar Tower Julich (STJ)', Germany [24]. This storage system is based on the redox cycle of Co_3O_4/CoO coated on the cordierite honeycomb structure, where air acts as the heat transfer medium as well as the reaction medium. The Authors have quantified the advantage of thermochemical storage concept and demonstrated that it offered almost double storage capacity in comparison with the same volume sensible-only storage system. Multi-cycling experiments also proved the performance reproducibility and showed very less degradation over the cycles.

Singh et al. [18] have modeled the same TCES reactor installed in the STJ facility. A two-dimensional axial-symmetric model based on the heat and mass balance and reaction kinetics governing the redox cycle of cobalt oxides has been developed. Validation against the experimental data from the STJ facility proved accuracy of the model to predict the thermal behavior of the storage for multiple redox looping cycles. This numerical model also allows better understanding of the complete thermochemical cycle and helps to identify the effect of variation of boundary conditions on the system.

In addition to the thermochemical materials, development of efficient and economical reactors/heat exchangers that can be integrated within the plant infrastructure is necessary for large-scale implementation of TCES systems. Mainly thermochemical reactors can be designed

in two configurations: Non-structured reactors such as packed beds, fluidized beds or rotary kilns; and structured reactors such as honeycombs.

The pilot-scale TCES system, installed in the above mentioned CSP plant STJ Germany is based on the Co_3O_4-coated honeycombs reactor. The study conducted by Tescari et.al [23] deals with design, construction, operation and overall feasibility of this TCES system. The packed bed reactor is the simplest reactor concept which is relatively easy to build and operate, but suffers from high energy losses due to the pressure drop. On the other hand, rotary kiln reactor configuration offers several advantages: uniform temperature on the internal wall, less irradiative heat losses due to the cavity shape, and high heat transfer between the particles and wall [13].

Neises et al. [25] have successfully demonstrated the feasibility of thermochemical heat storage through cobalt oxide powder inside a rotary kiln, based on the batch mode operation. This reactor achieved more than 50% conversion of oxides; however, the energy efficiency was limited due to high thermal capacitance of the reactor. This issue has been addressed by Tescari et al. [17] with a new optimized rotary kiln working in the continuous mode.

This literature survey shows that numerical analysis as well as experimental investigation of the TCES reactive materials and reactor design has been the research focus during past few decades. However, while sensible and latent heat storage systems have made their way into commercial applications, TCES is still at the laboratory stage, mainly due to technical challenges [26]. Therefore, simulations tools are essential to model the thermochemical reactions, understand the reaction kinetics and optimize the system performance. The present work is a contribution towards this effort that focuses on the TCES based on the redox cycle of cobalt oxides Co_3O_4 /CoO coated on the cordierite honeycomb.

The one-dimensional numerical model established in this work is based on the relations for the conservation of energy and kinetics governing the redox reaction, which are solved in the MATLAB environment. The model is validated against the experimental data obtained from the literature (Singh et al. [18]), as the TCES under study is still in designing phase and experimental data is not available at present. Parameter analysis is also carried out to investigate the influence of module structure and physical properties on thermal performance of the storage.

Overall, this simplified model allows simulating the thermochemical storage with reasonable accuracy and with less computational effort. This will be an innovative approach as the numerical model offers short computational time, thus it can be integrated with the CSP plant components in order to perform dynamic simulation of the whole CSP hybrid systems.

2. Mathematical model of Thermochemical Energy Storage (TCES)

The thermochemical storage under study is originally derived from a sensible heat storage system, which has been developed at the Zhejiang University, China. This system is based on the ceramics honeycomb constituting the storage column and air is the heat transfer medium, which is heated by an electrical furnace (Figure 1). Luo et al. [27] have also developed the numerical model to simulate the thermal performances of this system. After the experimental validation, the developed model has been applied for the parametric study to predict the effects of geometric and thermo-physical parameters on the TES performance.

Further, to achieve higher energy storage capacity and storage temperature within same volume size of the storage device, TCES system is proposed. Hence, next development in this project is designing of a TCES system based on the redox cycle of metallic oxides such as Co_3O_4/CoO or CuO/Cu_2O coated on the similar ceramics honeycomb. For this purpose, Thermogravimetric Analysis (TGA) of various metallic oxides is also being carried out to select the suitable oxides for thermochemical storage [28]. The modeling of a TCES prototype presented in this study is a contribution towards this work: optimize the storage performance and study the reaction kinetics of cobalt oxides before designing the actual TCES system.

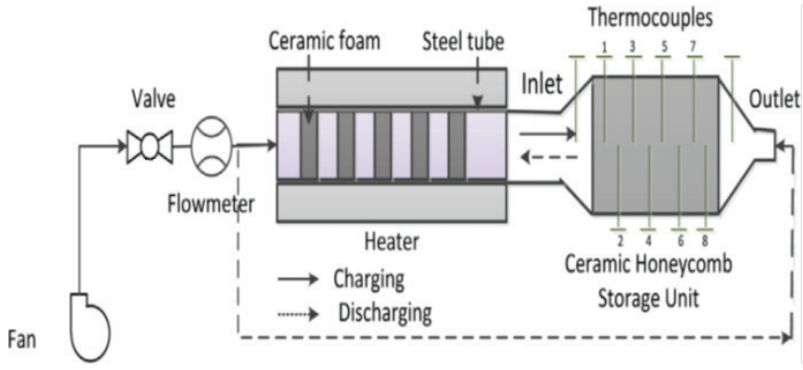

Figure 1 Schematic of experimental system at Zhejiang University (reproduced from [23])

Since experimental data from the TCES system at Zhejiang University are not available at present, authors have validated the present model against the experimental data obtained from the reference study for a similar system by Singh et al. [18]. They have modelled a TCES system based on the redox cycle of Co_3O_4/CoO coated on the cordierite honeycombs. Singh's model [18] is a 2D model based on the ANSYS-FLUENT, and it has been validated against the experimental data from the TCES prototype reactor installed at Solar Tower Jülich (STJ), Germany [24].

The model developed in this study is also validated against the same experimental results taken from the reference study [18]. Hence, same storage specifications and concentration of the reactive materials (Table 1) and schematic of the storage reactor from their experimental system are considered in the model (Figure 2a). Temperature and mass flow rate of the inlet air for the whole cycle taken from the reference study is also shown in Figure 2b.

Table 1 Specifications of the storage system

Total mass of the storage system (kg)	139
Initial mass of Co_3O_4 (kg)	44
Mass of cordierite (kg)	95
Initial fraction of Co_3O_4 inside the storage (-)	0.315
Hydraulic diameter of the channels (m)	0.007
Wall thickness of the channels (m)	0.002
Length of the storage reactor (m)	0.6

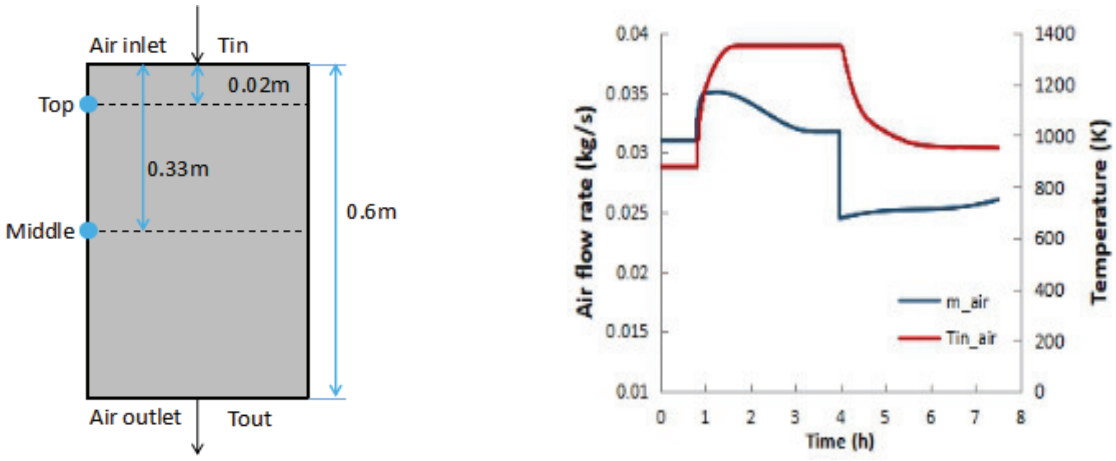

Figure 2 (a) Schematic of the storage reactor, (b) Inlet air temperature and mass flow rate for thermochemical storage cycle

Figure 3a shows the physical model of TCES under study: cordierite honeycomb is coated with reactive material Co_3O_4, and air as the heat transfer medium flows through the storage device during charging and discharging phases. Numerical model of TCES system is one-dimensional model, developed in the MATLAB environment. Figure 3b shows the simulation configuration discretized into M cells. The cordierite wall (grey layer) and reactants Co_3O_4/CoO (yellow layer) compose the solid layer in the model. The variable x is the distance from the air inlet of the flow channel. Air flows into the module at the boundary x=0 (i=1) and leaves at x=L (i=M+1). Energy balance and reactions kinetics are solved for each i^{th} cell using explicit scheme at each time interval j.

The model is based on the following assumptions:

- One-dimensional conduction in the flow direction.
- Adiabatic external wall without heat losses.
- Uniform initial mass of reactants (Co_3O_4) and initial solid temperature along the channels.
- Surface reaction and no diffusion effect in the reactants layer.
- Constant air mass flow rate (effect of change in oxygen concentration is neglected).

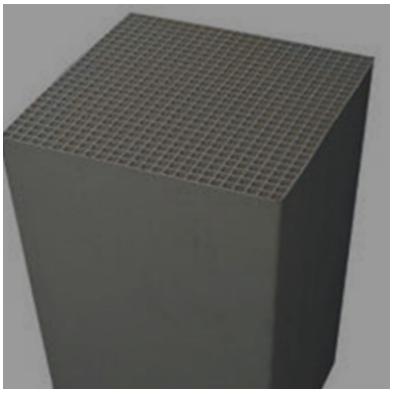

(a)

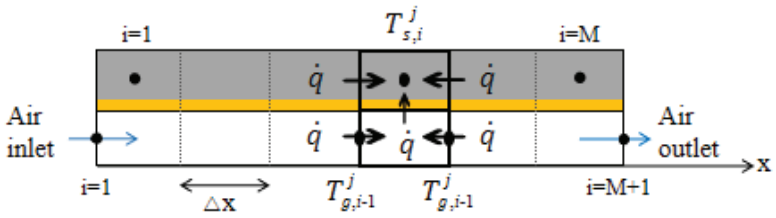

(b)

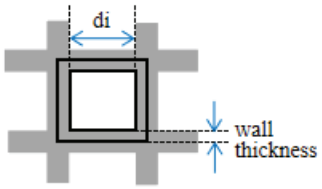

(c)

Figure 3 (a) Cordierite honeycomb coated with cobalt oxide, (b) Discretization scheme of the module in flow direction, (c) Hydraulic diameter and wall thickness of channels

2.1. Heat transfer

The heat transfer process involves conductivity of the solid material and convective heat transfer between air and solid surfaces. Solid and fluid are not in thermal equilibrium at any instant of the cycle, hence, thermal non-equilibrium separate energy equations are solved for each phase (Eqs.3 and 4). For one module, A_f is total air flow area of all channels and A_h is total heat transfer area of all channels. A_s is cross section area of the solid.

Solid:

$$\rho^j_{si} \cdot A_s dx \cdot C^j_{vi} \frac{Ts^{j+1}_i - Ts^j_i}{dt} = \lambda^j_i A_s \frac{Ts^j_{i-1} - 2Ts^{j+1}_i + Ts^j_{i+1}}{dx} + h^j_i A_c \left(\frac{Tg^{j+1}_i + Tg^j_{i+1}}{2} - Ts^{j+1}_i \right) + S^j_{hi} \cdot dx \quad (3)$$

Fluid:

$$\rho^j_{gi} \cdot A_f dx \cdot C^j_{vi} \frac{Tg^{j+1}_i - Tg^j_i}{dt} = \dot{m}_{i-1} C^j_{pi-1} Tg^j_{i-1} - \dot{m}_i C^j_{pi} Tg^{j+1}_i - h^j_i A_c \left(\frac{Tg^{j+1}_i + Tg^j_{i+1}}{2} - Ts^{j+1}_i \right) \quad (4)$$

According to Reynolds number calculation (Re<2000), the airflow is in laminar state, the empirical correlation of the convective heat transfer for laminar flow is given by Mills [29] (Eq.5):

$$Nu = 3.66 + \frac{0.065 \cdot Re \cdot Pr \cdot D/L}{1 + 0.04\,(Re \cdot Pr \cdot D/L)^{2/3}} \quad (5)$$

$$Nu = \frac{\mathrm{h} \cdot \mathrm{di}}{\lambda} \quad (6)$$

Considering the experimental conditions from the reference study by Singh et al. [18], the initial temperature of entire solid is kept at 875 K at the beginning of cycle. Boundary conditions like inlet air temperature and mass flow rate for thermochemical storage cycle is already shown in Figure 2b:

At t>0: $\mathrm{Ts} = 875\mathrm{K}(0 \leq x \leq \mathrm{L})$; $\mathrm{Tg} = \mathrm{Ts}(0 \leq x \leq \mathrm{L})$

At x=0, t>0: $\frac{\mathrm{dTs}}{\mathrm{dx}} = 0$; $\mathrm{Tg} = T_{in\_air}$; $m_{inlet} = m\_air$

At x=L, t>0: $\frac{\mathrm{dTs}}{\mathrm{dx}} = 0$; $\frac{\mathrm{dTg}}{\mathrm{dx}} = 0$

Thermodynamic properties of air is considered as temperature dependent and derived from NIST REFPROP database. The solid reactive material is the cordierite material coated with Co_3O_4. Hence, thermodynamic properties such as specific heat capacity, thermal conductivity and density of the reactive material depend on the mass fraction of cobalt oxides (φ) in the total solid material, reaction advancement (*f)* and properties ($\emptyset$) of both cordierite and cobalt oxide specie *i.* Hence, each physical property of the reactive material is calculated according to following relation (Eq.7) [16]:

$$\emptyset = \varphi \cdot \sum_i (f_i \cdot \emptyset_i) + (1 - \varphi) \cdot \emptyset_{corderite} \quad (7)$$

Where *i* denote the respective cobalt oxide species. The specific thermodynamic properties of solid materials are derived from previous work of Singh et al. [18].

2.2. Reaction kinetics

The redox reaction kinetic model of Co_3O_4/CoO implemented in this study is developed by Singh et al. [18]. It's based on the model originally derived by Pagkoura et al. [30], which was created from the experiments using flow through pellets of Co_3O_4 in the temperature range of 1073–1273 K. Afterwards, this kinetic model was extrapolated for temperatures outside this

temperature range by Singh et al. [18]. In actual, the kinetic model fitting parameters (E_{red} and E_{oxi}) are varied to get optimum fit to the experimental data.

The redox reaction is considered to interact thermally with the solid material, as it absorbs heat from the solid during the reduction step and supplies heat to it during the oxidation step. Hence, in the numerical model, a heat source term S_h is integrated in the energy equation for solid medium (Eq.3). In this study, it is simplified as a function of the reaction rate R and concentration C of the reactive species at any time instant t, and overall reaction enthalpy ΔH_r (Eq.8):

$$S_{h(t)} = \Delta H_r \cdot R_t \cdot C_t \tag{8}$$

2.3. Cell number and time step

The effect of time step and cell number (element number) M on computation time and simulation result is also studied. The total energy stored in charging process $Q_{charging}$ and total energy released in discharging process $Q_{discharging}$ are the reference parameters. As shown in Table 2, when M is more than 60, relative change in these reference parameters is very small. Table 3 and Figure 4 compare the simulation results of different time step. When time step is reduced to 0.1s, computation time increases by 100 times as much as that of 10s but the relative change of $Q_{charging}$ and $Q_{discharging}$ is marginal. Therefore, cell number 60 and time step 10s are chosen in this study. The simulations have been performed on 8 core CPU.

Table 2 Simulation results of different cell number M (time step=10s)

M	20	60	80	100	120
$Q_{charging}$ (MJ)	115.292	115.27	115.268	115.267	115.267
$Q_{discharging}$ (MJ)	93.394	93.307	93.298	93.296	93.295
Computation time (s)	173.3	510.2	672.1	833.2	1018.7

Table 3 Simulation results of different time steps (M=60)

Time step (s)	0.1	2	10	20	30	40
$Q_{charging}$ (MJ)	116.055	115.756	115.27	114.338	113.459	112.629
$Q_{discharging}$ (MJ)	93.48	93.414	93.307	93.055	92.794	92.514
Computation time (s)	50990.5	2573.3	510.2	255.1	172.2	129.2

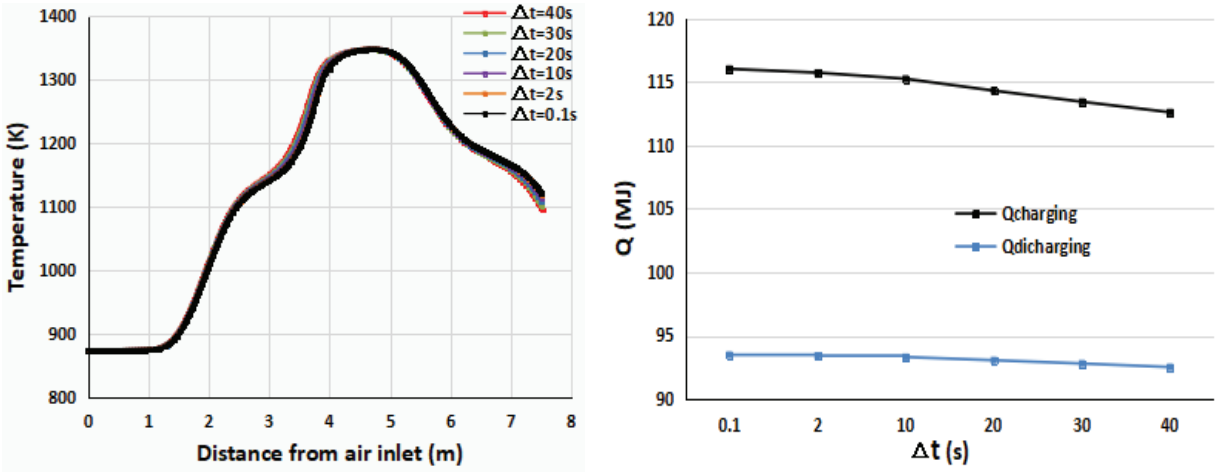

(a) **(b)**

Figure 4 (a) Outlet air temperature profiles with different simulation time steps, (b) Total Energy in charging and discharging process with different simulation time steps

3. Results and discussion

3.1. Thermal behaviour of TCES

In the beginning, the high temperature inlet air transfers heat to the solid material leading to an increase in solid temperature (sensible storage). When solid temperature approaches the reduction temperature of Co_3O_4 (around 1164 K at 1 bar pressure), the reaction starts (Eq.9) and the heat transferred from the air to solid is absorbed by the endothermic reaction (chemical storage). Solid temperature remains almost constant (plateau formation). When the chemical reaction reaches completion, the energy is again stored in its sensible form, and solid temperature starts rising.

Charging (reduction): $$Co_3O_4 \xrightarrow{\Delta H_r} 3CoO + 1/2O_2 \quad (9)$$

During discharging, cold air flows through the storage. In the beginning, the solid material releases heat to the air in sensible form, thereby cooling down the solid until the oxidation temperature of CoO (around 1164 K at 1 bar pressure) is reached. During oxidation, inlet air is heated up using energy of the exothermic reaction (Eq.10) and solid temperature remains almost constant resulting in plateau formation. After completion of the oxidation, sensible heat from the solid is again released to the air until the solid temperature decreases to the inlet air temperature.

Discharging (oxidation): $$3CoO + 1/2O_2 \overset{\Delta H_r}{\rightarrow} Co_3O_4 \quad (10)$$

Figure 5 shows the comparison between experimental results and simulation results of this work for temperature at the middle and top of the storage device and the outlet air temperature (see Figure 2), during a complete redox cycle. Dashed lines represent experimental results from the reference study [18], and solid lines represent results obtained from the developed model. According to the measurement position in the experiment, top position (Ts_top) corresponds to x=0.02 m and middle position (Ts_middle) corresponds to x=0.33 m. It can be observed that generally simulation results are in good agreement with the experimental results except some discrepancies. The maximum deviation of outlet air temperature is in the 8-10% range. The temperature curve shows especially large discrepancy in discharging process and the maximum deviation of solid temperature between the simulation and experimental results is around 4.3%.

The main reason causing the deviation from the experimental results is the neglection of heat loss at the external boundaries of the storage system. This led to a higher peak value of solid temperature (1350K) than that in the experiment in Figure 5a. It is also evident in Figure 5a that, the discrepancy grows when the temperature of storage module is above 1150K, which might be caused by more radiation heat loss in the experiments. Figure 5b compares the two outlet air temperature calculated by 1-D model of this study and the 2-D model of the reference paper [18]. According to reference study [18], the bottom of the reactor suffered from relatively high heat loss than the lateral walls of the reactor, which makes the outlet air temperature measured in the experiments unreliable enough, so only the outlet air temperature calculated by their 2-D model is given. A higher peak value of the outlet air temperature (~1325K) could also be seen from the

1-D simulation result. Overall, the outlet air temperature of 1-D model is more discrepant from the referenced result due to the more heat loss at the bottom of the reactor in the experiment.

Furthermore, the reaction kinetic model might not exactly match with the experimental conditions because the two temperature plateaus (reaction periods) shown by the simulation results are shorter than those of experimental results.

Moreover, one-dimensional model in the present study neglects the heat transfer effect at radial direction , as well as, it might not take into account the concentration or distribution of reactive species in the whole storage more accurately, which can affect the overall reaction rate and consequently thermal behaviour of the storage. As for other boundary conditions, trend of the air mass flow captured by the numerical equations and provided as input to the model, might not be so accurate due to high fluctuations in the real experiments [18]. Despite of the discrepancies clarified as above, the established model can reasonably predict the overall trend of the thermochemical storage system.

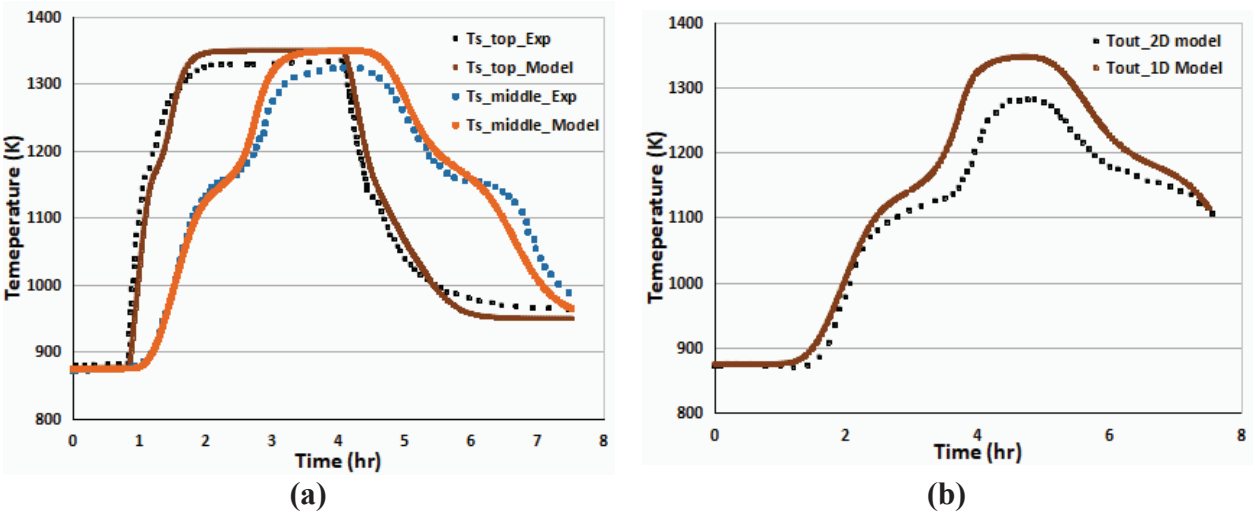

Figure 5 Comparison of temperatures between the 1-D model and referenced study [18]: (a) top and middle solid temperature, (b) outlet air temperature

Figure 6 shows the solid and air temperature distribution along the channel at different time intervals. At the end of charging process, solid temperature along the channel (x<0.5m) almost reaches the highest value 1350 K while the solid close to the air outlet (0.5m<x<0.6m) has lower temperature. As is seen in Figure 6*b*, cold air can be quickly heat up within 0.6 m and the

temperature difference between solid and air at the outlet is very small. This explains why there is no obvious drop in outlet air temperature at the beginning period of discharging process (4 hr~4.8 hr). Afterwards, with the lower inlet air temperature, solid temperature continuously decreases and outlet air temperature also drops.

The reaction period is also revealed by the fluctuation of the temperature curves in Figure 6. During charging process (Figure 6*a*), the temperature curves at 2 hr is slightly concave where 0.1 m<x<0.3 m because of the reduction of Co_3O_4. This is because the endothermic reaction slightly decelerates the temperature change as heat from inlet air is absorbed by the endothermic reaction. When chemical reaction approaches to completion, the temperature curves resume the trend. The same case with convex shape of temperature curves in discharging process at 6hr (Figure 6*c*) which is caused by the oxidation of CoO, when inlet air is heated up using energy of the exothermic reaction.

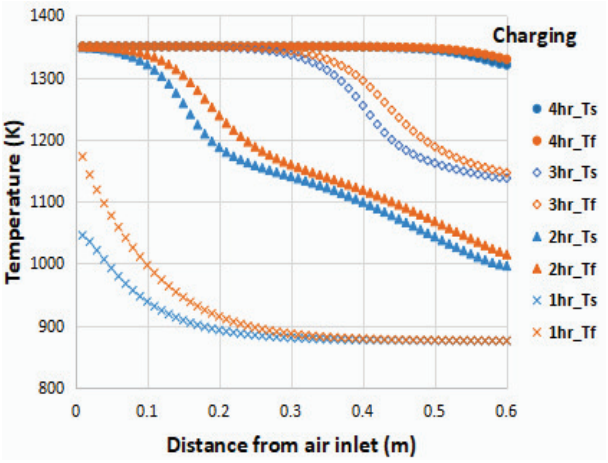

(a)

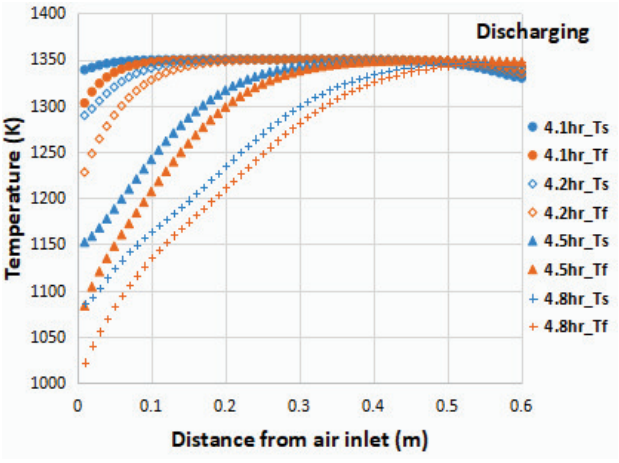

(b)

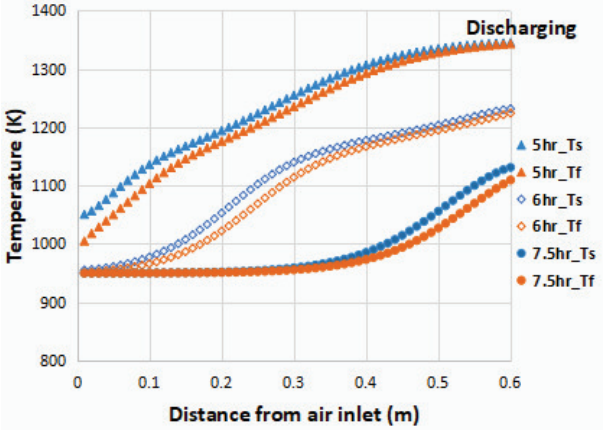

(c)

Figure 6 Solid and air temperature distribution along the channel during the redox cycle: (a) charging process (0hr~4hr), (b) discharging process (4hr~4.8hr), (c) discharging process (5hr~7.5hr)

3.2. Conversion of cobalt oxides

The concentration of reactive species changes as the reaction proceeds. During charging, initially concentration is constant, until the solid achieves the reduction temperature. Afterwards, the Co_3O_4 concentration decays as the reduction proceeds and produces CoO. When the reduction is complete concentration of both oxides again becomes constant (Figure 7). Likewise, during discharging, when solid cools down to the reaction temperature, oxidation of CoO initiates and produces Co_3O_4. When the oxidation is complete concentration of both species again becomes constant. Figure 7 demonstrates the concentrations change of cobalt oxides during the complete redox cycle. Since temperature at the top of the storage (closer to the inlet) rises earlier, hence reaction at the top starts earlier (Figure 7a) in comparison with middle and bottom of the storage which achieve reaction temperature later (Figure 7b and 7c). According to Figure 7, the redox of Co_3O_4 along the channels is almost complete under the specific conditions.

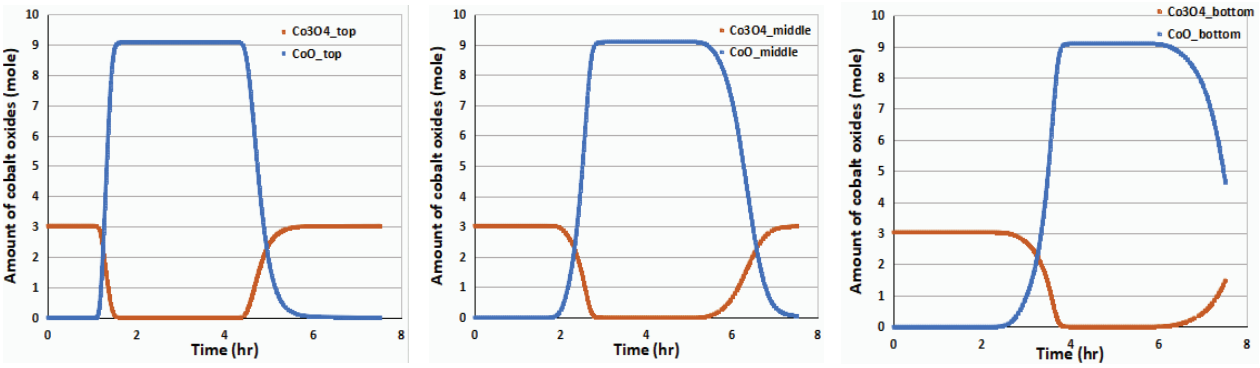

(a) **(b)** **(c)**

Figure 7 Conversion of cobalt oxides during the redox cycle: (a) top, (b) middle, (c) bottom of the storage

3.3. Energy balance

The total energy stored/released in a TCES system is given as (Eq.11) [23]:

$$Q_{stored} = \int_0^t \dot{m} \cdot (h_{in} - h_{out}) \mathrm{dt} \quad (11)$$

Where t is the total time for charging or discharging process; h_{in} is the specific enthalpy of air at the inlet; h_{out} is the specific enthalpy of air at the outlet; $\dot{m}$ is the total mass flow rate.

The chemical heat storage depends on the reaction enthalpy (ΔH_r) and change in concentration of the reactive species from the beginning to the end of the cycle, over the entire length of the storage (L) (Eq.12):

$$Q_{chemical} = \int_0^L \int_0^t \Delta H_r \cdot \Delta M_{Co_3O_4} dt dl \quad (12)$$

Where ΔM_{Co3O4} is the concentration difference of Co_3O_4 (*moles*) between consecutive time intervals (Δt) of one cell.

Sensible heat storage ($Q_{sensible}$) is calculated as (Eq.13):

$$Q_{sensible} = Q_{stored} - Q_{chemical} \quad (13)$$

The relative percentage error from the experimental results of the energy stored/released in the storage system is calculated as (Eq.14):

$$\varepsilon_{rel} = \frac{|Q_{model} - Q_{exp}|}{Q_{exp}} \times 100 \quad (14)$$

Table 4 shows the total energy (sensible as well as chemical) stored/released from the TCES, and relative percent error between simulation and experimental results. It can be observed that at the end of discharging, temperature of the storage is still higher than initial temperature at the beginning of charging phase (Figure 5a); hence, some of the energy is still retained by the solid and is not discharged so the energy released in discharging process is less than the energy stored. Although the lateral walls of the storage device are well insulated in the experiment and thus the temperature profiles show good agreement in Figure 5, the bottom of the reactor suffered from relatively high heat loss [18], therefore, the heat loss amount should be considered in the validation of the energy amount. According to some other experiments of thermochemical storage conducted by DLR [23], it is assumed that heat loss accounts for 18% of the total energy stored/released in the experimental storage system under ideal conditions ($Q_{exp,ideal}$), so $Q_{exp,ideal}$ can be calculated from the real total energy stored/released in the experimental storage system

($Q_{exp,real}$). The percentage relative deviation between $Q_{exp,\ ideal}$ and $Q_{model,\ ideal}$ is 7.42% and 19.60%, for charging and discharging, respectively. One possible reason for the simulation error could be the neglecting the flow non-uniformity at the radial direction, which would cause the central air flow rate to be larger than that of the edge part in one module. With uneven flow distribution, the heat transfer process would be deteriorated in those channels at the edge part of the module and there would be less amount of energy stored or released. These error values are acceptable considering that the energy storage systems are summing calculation errors over time. Thus, as mentioned above, bigger errors for the temperature calculation of discharging process generate larger amount of percentage relative errors in the stored energy [6].

Table 2 Total energy stored/released during the redox cycle from TCES

		Charging	**Discharging**
$Q_{exp,real}$ (MJ)		87.993	63.978
$Q_{exp,ideal}$ (MJ)		107.309	78.022
$Q_{model,ideal}$ (MJ)	Chemical	35.711	33.243
	Sensible	79.559	60.064
	Total	115.27	93.307
η_{rel} (%)		7.42	19.60

Figure 8 compares the solid and outlet air temperature of the thermochemical storage with those of a pure sensible heat storage system. The sensible heat storage model is based on the pure cordierite honeycomb with the same total mass of 139 kg, geometry structure and inlet air conditions are same as for the thermochemical storage.

It is observed that chemical reactions prolong the charging and discharging period because part of the heat transferred between the solid and fluid is stored or released in the form of chemical energy, thus both the change of solid and air temperature are slower in comparison with the sensible heat storage phase (Figure 8). Energy stored in the pure sensible heat storage system during charging is about 96.072 MJ (16.65% less than that of thermochemical storage) and the energy released during discharging is 79.841 MJ (14.43% less than that of the thermochemical storage). Hence, the thermochemical storage system is capable of achieving higher energy density as compared to the pure sensible heat storage system.

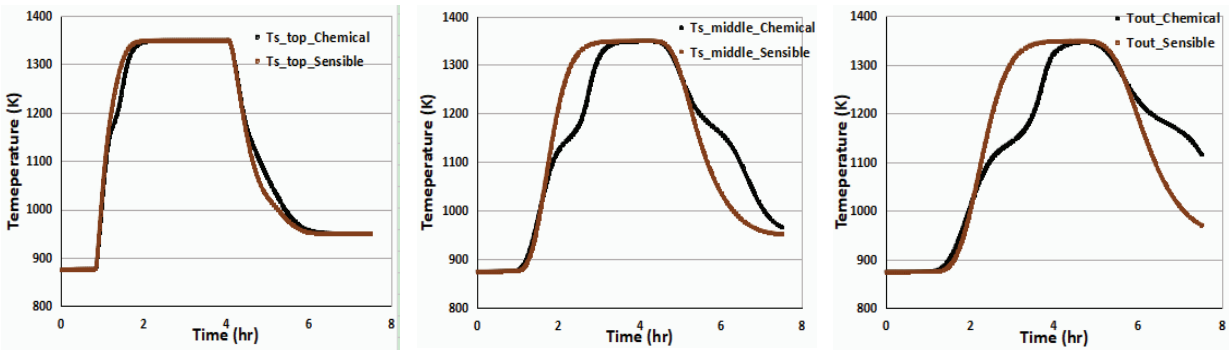

Figure 8 Comparison of temperatures between the sensible heat storage and thermochemical heat storage: (a) top solid temperature, (b) middle solid temperature, (c) outlet air temperature

3.4. TCES cycle

In order to demonstrate the whole cycle of thermochemical storage, different stages have been marked on the solid temperature curve at x=0.33 m (Figure 9). The temperature plateau during each phase is the characteristic of thermochemical storage systems. The width of the plateau (about 40 min for charging and 56 min for discharging at x=0.33 m) is positively correlated with the chemical energy stored inside the storage system and is greatly affected by the temperature change rate at every position.

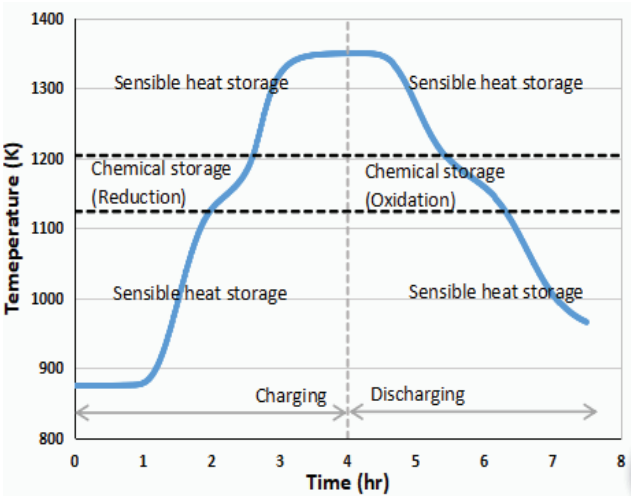

Figure 9 Stages of thermochemical storage during the redox cycle

4. Parametric study for Thermochemical Energy Storage

The developed model is applied to perform the parametric study to analyse the impact of material properties and reaction kinetics on the thermochemical storage. For this analysis, the same initial concentration (total solid mass of cordierite honeycomb and cobalt oxides) and inlet air conditions are assumed as in the experiment, and cobalt oxides are totally converted during their reaction period (charging period is 4 hours and discharging period is 6 hours).

4.1. The effect of specific heat of storage material

Specific heat of the storage material is an important parameter for thermal capacity of the storage system when mass of the storage materials is constant. Figure 10a shows effect of the specific heat of the solid material on the outlet air temperature. Although larger specific heat results in higher energy storage, it also decelerates the change in outlet air temperature. Air outlet temperature increased to 1350 K in 4 hours when specific heat was 900 J/kg-K, and reached up to 1280 K with 1500 J/kg-K specific heat within same time period. With smaller specific heat, outlet air temperature dropped a little more quickly during discharging, while higher specific heat resulted in more gradual heat release.

Rate of redox reaction is also effected by specific heat; Co_3O_4/CoO inside the whole storage system could be totally reduced or oxidized in charging or discharging periods with smaller specific heat, but it takes longer time in case of larger specific heat. The reduction period is 45 minutes shorter when specific heat was 900 J/kg-K as compared with 1500 J/kg-K (Figure 10b).

The mass conversion rate of Co_3O_4 inside the whole storage system is shown in Figure 10c, that is the whole reaction rate based on the mass of Co_3O_4. The negative value represents the reduction period and the positive value indicates the oxidation process. The integration of this rate with time (area between the curves and time axis) should be same for the three cases because total mass of Co_3O_4 is the same in all cases. Therefore, the maximum reaction rate of the storage system with the smallest specific heat is the highest in both charging and discharging process. Actually, the highest reaction rate of the storage is due to the shortest reaction period resulted from the highest rate of temperature change when specific heat was 900 J/kg-K.

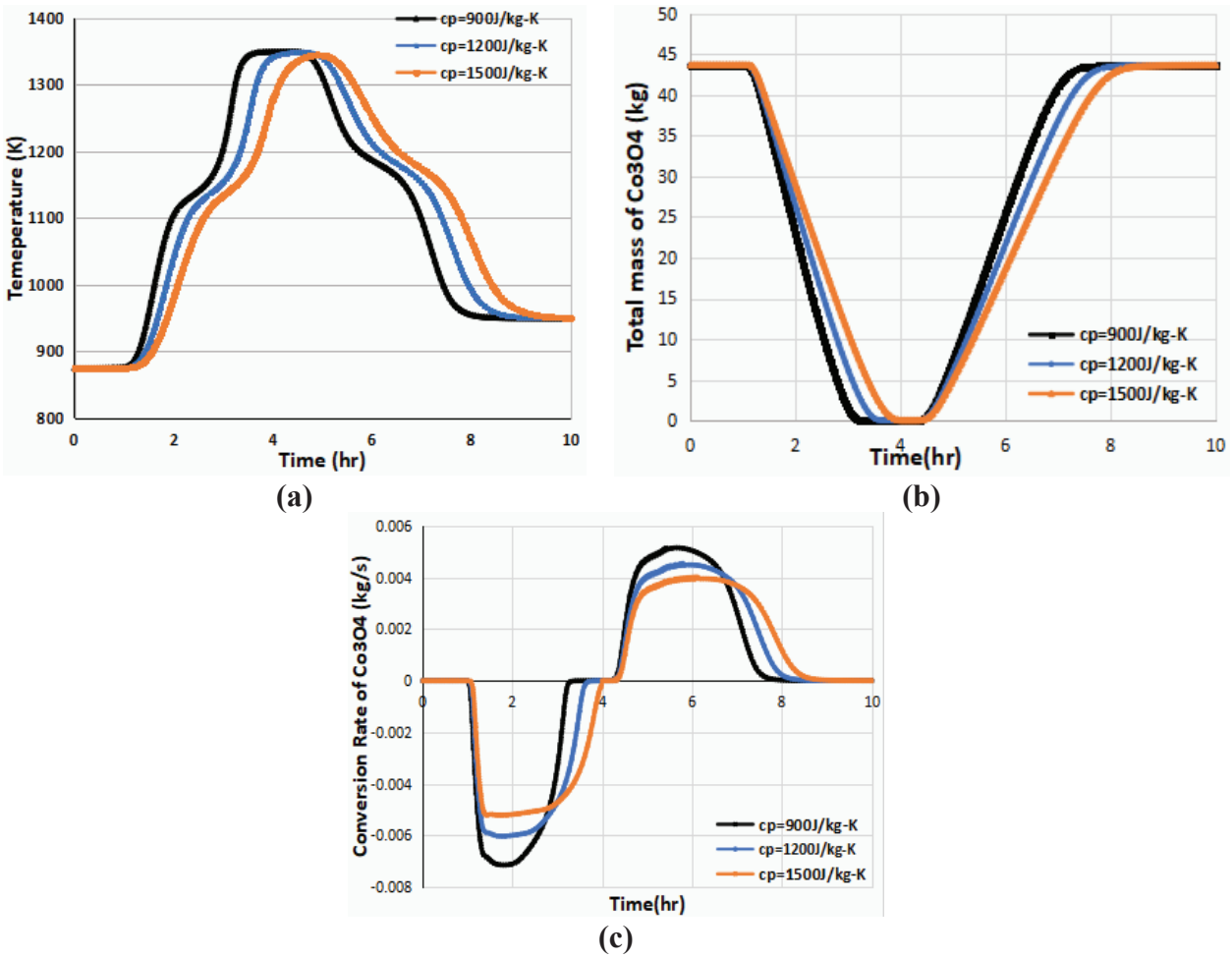

Figure 10 (a) Effect of specific heat capacity on the air outlet temperature, (b)Mass conversion of Co_3O_4 in charging and discharging periods, (c)Mass conversion rate of Co_3O_4 in charging and discharging periods

4.2. The effect of channel wall thickness

Figure 11a shows the influence of different wall thickness of the channels on air outlet temperature, when inner diameter of the channel is fixed at 0.007 m. During charging process, air outlet temperature changes more gradually and reaches to lower peak value for larger wall thicknesss: air temperature reached up to 1350 K within 4 hours for 0.001 m thick wall and up to ~1300 K for 0.004 m thick wall. This trend is also obvious in discharging and complete discharging period is longer for larger wall thickness.

Smaller wall thickness leads to larger channel density in the storage module when inner diameter and total solid mass are constant. Total heat transfer area A_c is larger while air speed is lower due

to the smaller air flow area A_f. The total heat transfer area A_c of 0.001 m-thick wall system is about 3.75 times as large as that of 0.003 m-thick wall system. As is shown in Figure 11c, average air speed inside the channels is within the range of 0.5~5m/s and Reynolds number is about 45~170 in laminar range. Although 0.003 m-thick wall system has an air speed 3 times bigger than that of 0.001 m-thick wall system, both the heat transfer coefficient h are around 32 W/m^2-K when Nusselt numbers calculated by Equation (5) are almost constant. Therefore, with the larger heat transfer area Ac, the thinner wall system has a larger average temperature change rate of outlet air temperature during the whole charging or discharging process.

It is noticed that outlet air temperature of the thicker wall system increases earlier at the beginning of charging period (1h~1.5h) and also decreases earlier at the beginning of discharging period (4.5h~5.5h), while there is a little time delay for the thinner wall system. Due to the smaller heat transfer area A_c of thicker wall module, when air flows from the inlet to the outlet, heat transferred from the hot air to the solid (charging) or from the high-temperature solid to cold air (discharging) is less than that when air flows through the thinner wall module of the same length L, so the temperature decrease of hot air (charging) or temperature increase of cold air (discharging) along the flow direction is smaller. At the outlet, air temperature of thicker wall module is higher (charging) or lower (discharging) than that of thinner wall module. Therefore, the increase or decrease of air temperature is first seen at the outlet of thicker wall module. This can be proved in Figure 12, which shows the air temperature distribution inside the module at different time (1h/1.5h/2h/3.5h). At 1.5h, the outlet air temperature of 0.003m-thick wall module first increases from 875K to 930K, while for 0.001m-thick wall module, outlet air temperature almost remains at the initial value 875K. During the period 1h~2h, the increase rate of air outlet temperature for thicker wall module is always the largest. It is also the same at the beginning (4.5h~5.5h) of the discharging process.

The reaction rate of the whole storage system based on mass of Co_3O_4 is presented in Figure 11b. The more quickly temperature increases or decreases, shorter the reduction or oxidation period are. It seems that the effect of wall thickness on the reaction period is not as significant as that of specific heat capacity. The reaction rates are almost the same during charging or discharging process for three different wall thicknesses. Moreover, it can be observed from both Figures 10c

and 11b that reduction rate of Co_3O_4 during charging period is generally higher than the formation rate of Co_3O_4 during discharging.

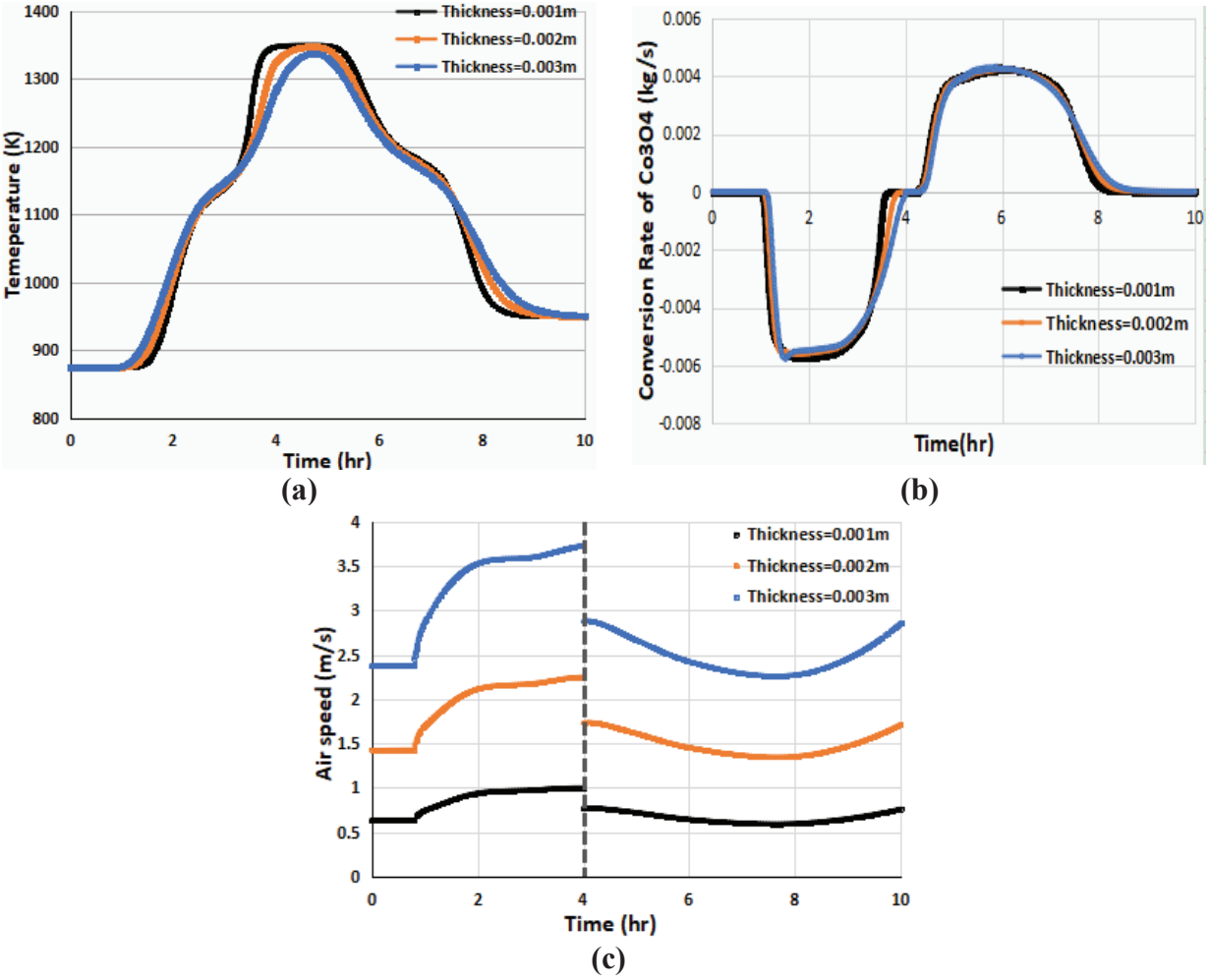

Figure 11 (a) Effect of wall thickness on the air outlet temperature, (b) Mass conversion rate of Co_3O_4 in charging and discharging periods, (c) Average air speed inside the storage module

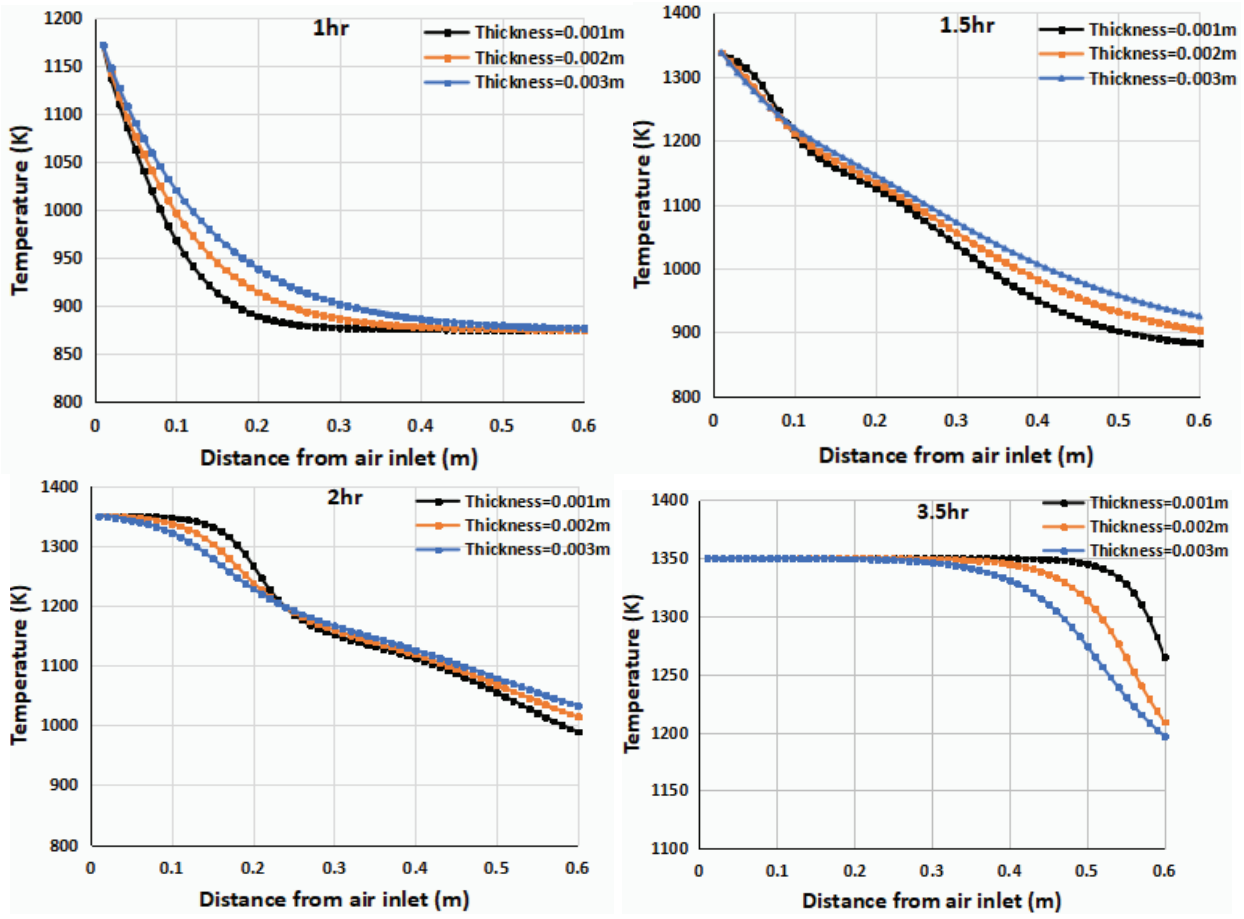

Figure 12 Air temperature distribution inside the module at 1h/1.5h/2h/3.5h

4.3. The effect of channel hydraulic diameter

The influence of hydraulic diameter of the channels on the air outlet temperature is shown in Figure 13a, when wall thickness of the channel is fixed at 0.002 m. When wall thickness and total solid mass are the constant, the smaller inner diameter leads to larger channel density but smaller air flow area A_f. As is shown in Figure 12d, the average air speed inside the module of 0.003m inner diameter is about 3 times larger than that in the module of 0.009m inner diameter. The Reynold numbers for three cases are within the range of 96.56~131.68. On the one hand, according to Equation (6), heat transfer coefficient h increases with smaller inner diameter of channels when Nusselt number is almost constant (3.685~3.716). On the other hand, heat transfer area A_c decreases with smaller diameter. Consequently, the larger effect comes from h, as shown by Figure 13b, the thermal resistance ($1/hA_c$, K/W) decreases with smaller diameter, so

heat transferred between solid and air within the same period is larger and the slope of outlet air temperature curve is larger (Figure 13a), which means the average heat transfer rate is larger during the whole charging and discharging process.

Furthermore, the outlet air temperature starts to increase (charging) or decrease (discharging) a bit earlier in the module of larger *di* which has smaller *h*. Due to the smaller *h*, when air flows from the inlet to the outlet in the module of larger *di*, less heat is transferred from the hot air to the solid (charging) or from the high-temperature solid to cold air (discharging) than that when air flows through the module of smaller *di* from the inlet to the outlet. Therefore, the temperature decrease of hot air (charging) or the temperature increase of cold air (discharging) is smaller from the inlet to the outlet in the module with larger *di*. As can be seen in Figure 14, at the beginning period of charging (1h~1.5h), the outlet air temperature of the module with di=0.009m is always larger than that of the module with di=0.003m. At 1.5h, the outlet air temperature of the module with di=0.009m first increases from 875K to 920K, while for the module with di=0.003m, the outlet air temperature almost remains at the initial value 875K. As is analyzed above, smaller channel diameter and smaller wall thickness have the similar effect on both the outlet air temperature and chemical reaction periods, but the former effect is less significant.

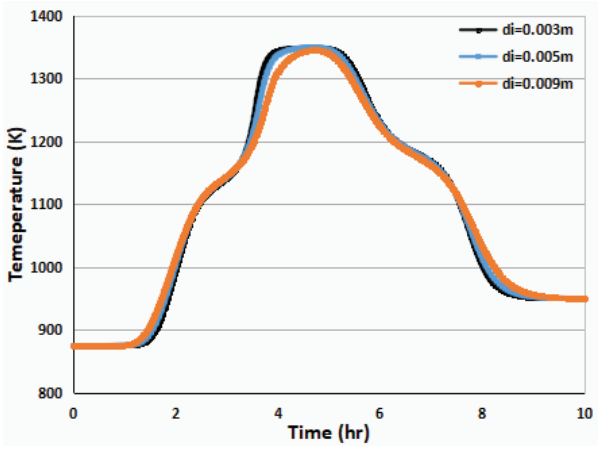

(a)

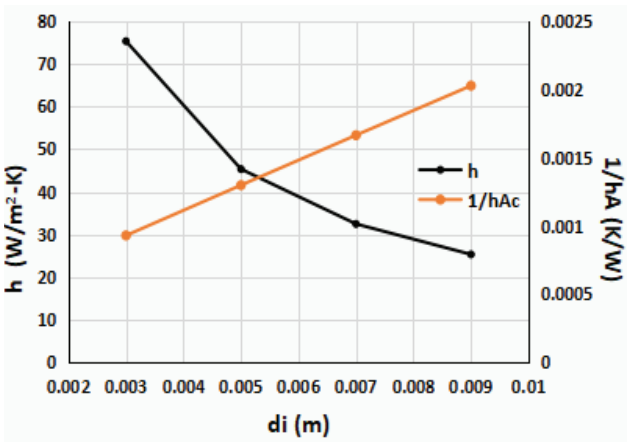

(b)

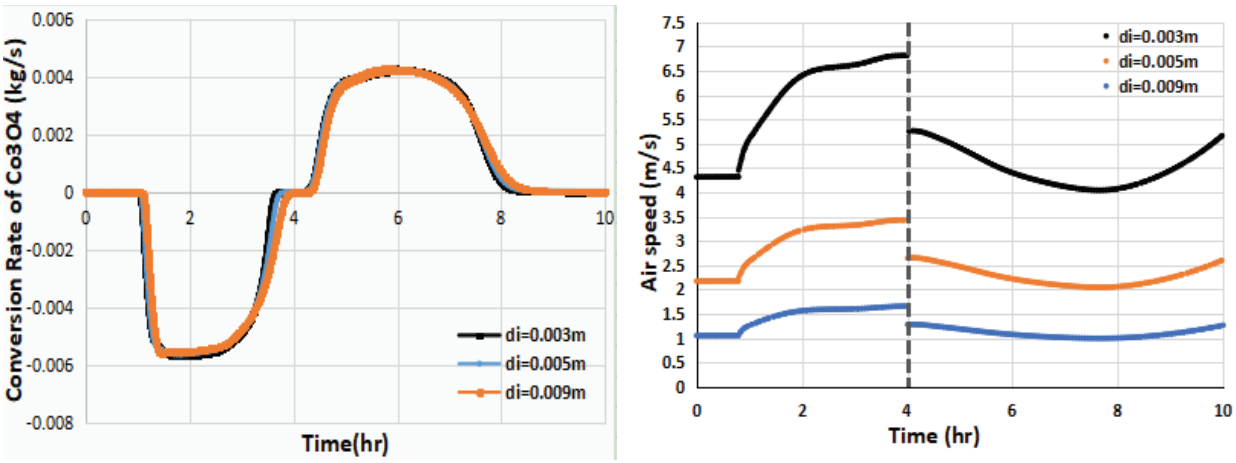

(c) (d)

Figure 13 (a) Effect of channel diameter on the air outlet temperature, (b) Heat transfer coefficient of different inner diameter cases, (c) Mass conversion rate of Co_3O_4 in charging and discharging periods, (d) Average air speed inside the storage module

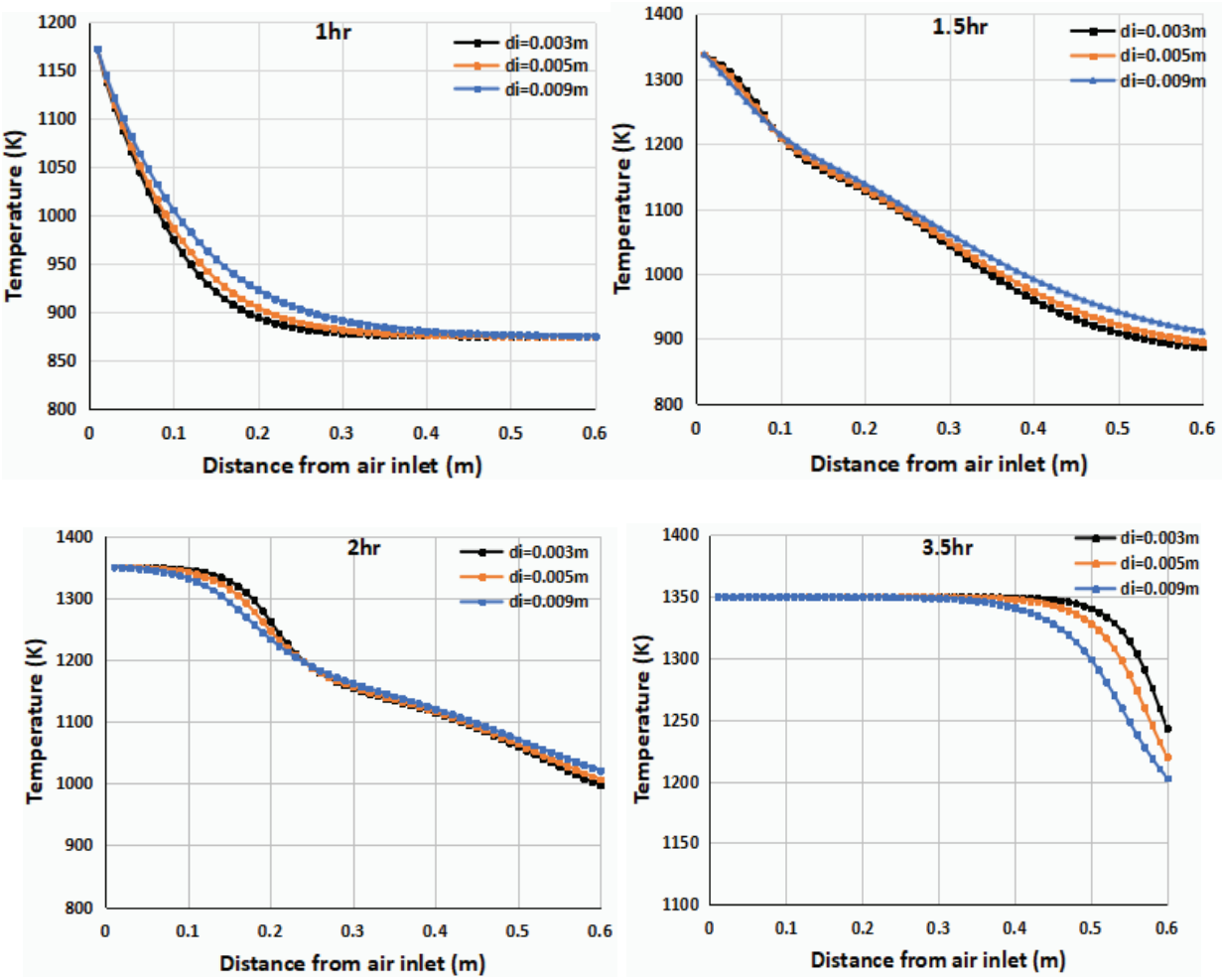

Figure 14 Air temperature distribution inside the module at 1h/1.5h/2h/3.5h

4.4. The effect of heat transfer coefficient

Another consideration about the heat storage system is the volume. It is better to have higher heat transfer coefficient (h) in order to make the storage volume smaller. Assuming the value of heat transfer coefficient in the previous validation case is $1h$, thus $2.5h$ and $5h$ represent the case where heat transfer coefficients are 1.5 times and 4 times larger with the same other conditions. Figure 15 demonstrates the outlet air temperature with different h and conversion rate of Co_3O_4. Likewise, larger h leads to the shorter charging or discharging period and reaction period because of higher heat transfer rate.

The method to increase the heat transfer coefficient mainly lies in improving the inner structure of honeycombs. For example, converging-diverging channels not only has larger heat transfer surface but also enhance the fluid turbulence so the heat transfer rate is greatly improved in comparison with straight channels [31]. Other common methods for heat transfer intensification, such as pin-fins channel, twisted channel, are difficult to be made inside the honeycombs and not very suitable to support the chemical reactants. Given the effect of heat transfer coefficient on the heat storage process and processing the thermochemical storage modules, the straight channel is more favorable.

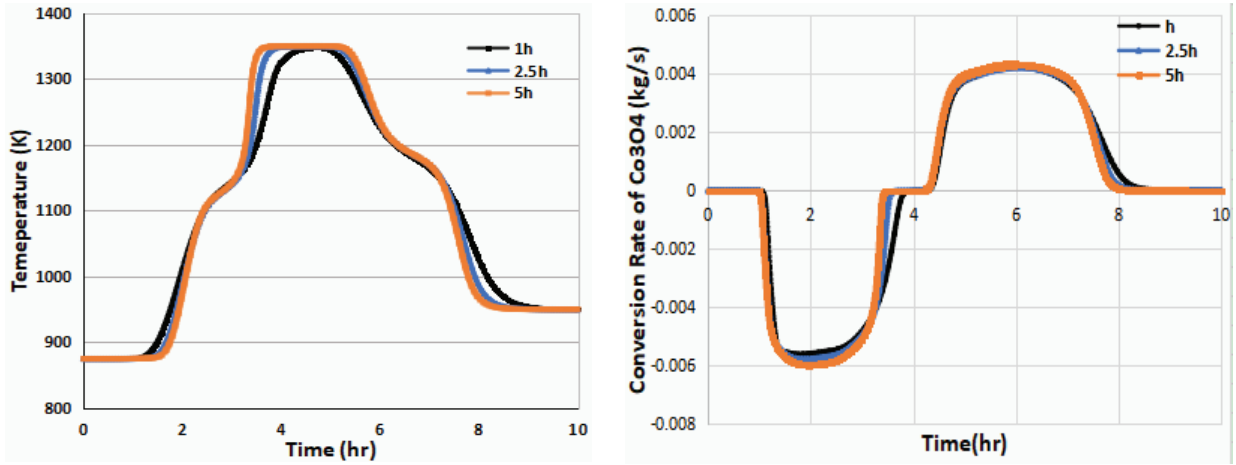

Figure 15 (a) Effect of heat transfer coefficient on the air outlet temperature, (b) Mass conversion rate of Co_3O_4 in charging and discharging periods

5. Conclusion

Thermochemical Energy Storage (TCES) systems have potential of high energy density, possibility of long-term storage and higher temperature range. However, this technology is still developing in comparison with sensible and latent heat storage systems, which have been developed on the commercial scale. In this study, a one-dimensional model for thermochemical storage based on the redox cycle of Co_3O_4/CoO pair is developed and presented. The mathematical model is based on the energy balance and reaction kinetics for the cobalt oxides. The developed model is validated against the experimental data obtained from the literature [18]. From this study, it is concluded that one-dimensional numerical model can reasonably predict the overall trend of thermochemical cycle, except some discrepancies (outlet air temperature deviations: <4% on average, <10% maximum; solid temperature deviations: <2% on average, <4% maximum).

Total energy stored/released from the TCES is also calculated using the model, and compared with the experimental results. Considering the heat loss of 18% of the total energy stored/released in the storage system, the percentage relative error between simulation and experimental results is 7.42% and 19.60%, for charging and discharging, respectively. Considering a pure sensible heat storage system with the same solid mass, the heat stored and released is about 16.65% and 14.43% less than that of the thermochemical heat storage system, respectively.

This model can be used to study the process of thermochemical storage, understand the reaction kinetics and investigate the capability of cobalt oxides to store thermochemical energy, with less computational effort. The parametric study is conducted when total mass of the storage materials is constant, which provides guidance to optimize the system performance within practical constraints:

- The specific heat of the solid materials (support materials and reactants) has the greatest impact on both the outlet air temperature and solid temperature. The larger heat capacity leads to higher energy storage but it delays and decelerates the temperature change during charging and discharging periods.

- Different channel wall thickness and inner diameter actually determines the heat transfer coefficient and heat transfer area of the whole storage module. Smaller wall thickness and inner diameter result in smaller total heat transfer resistance (*1/hA*, K/W), therefore, both the outlet air temperature and solid temperature change more quickly within the same charging and discharging periods. The effect of wall thickness is more significant than the inner diameter. Given the small effect of heat transfer coefficient on the heat storage process, it is better to design the structure of storage module which is both easier to manufacture and can support the reactants, like honeycombs with straight channels.
- The temperature change rate of solid reactants (Co_3O_4/CoO) affects chemical reaction period and reaction rate. With larger temperature change rate during the charging and discharging process, the reaction period is shorter and the maximum reaction rate is also higher. The effect of wall thickness on the chemical reaction period is not as significant as that of the specific heat. Generally, the reduction rate of Co_3O_4 during charging period is higher than the formation rate of Co_3O_4.

Future work will focus on the design and optimization of a pilot scale TCES for CSP hybrid systems and integration of TCES model in the whole system dynamic models for CSP hybrid systems.

Acknowledgment

The authors gratefully acknowledge the support from (1) National Key R&D Program of China (NO.2016YFE0124700), (2) the National Natural Science Foundation of China (NO.51776186 and 51621005), and (3) Zhejiang University China for supporting researchers exchange within the Program of Introducing Talents of Discipline to University on Energy, Science and Technology (Project 111, NO.B08026).

Nomenclature

A	Frequency factor in Arrhenius equation (s^{-1})	*h*	Heat transfer coefficient (W /m^2-K)
A_c	Total heat transfer area (m^2)	ΔH_r	Reaction enthalpy (J/mol)
A_f	Total air flow area (m^2)	*K*	Reaction rate constants (-) (1-reduction, 2-oxidation)
A_s	Total solid cross section area(m^2)	*M*	Moles

c_p	Specific heat (J/kg-K)	Q	Energy (J)
C	Concentration of reactants (mole/m)	R	Universal gas constant (J/mol-K)
d	Diameter (m)	S_h	Heat source term (W/m)
E	Kinetic model fitting parameter (K)	T	Temperature (K)
f	Fraction of cobalt oxide species (-)	u	Velocity (m/s)
Greek letters			
ρ	Density (kg/m^3)	φ	Fraction of Co_3O_4 in total solid material (-)
λ	Thermal conductivity (W/m-K)		Reletive percentage error
Subscripts			
f/g	fluid/air	*s*	solid
red	reduction	r	reaction
oxi	oxidation	i	internal
rel	reletive		

References

1. Rivarolo M., Cuneo A., Traverso A., Massardo A.F., Design optimisation of smart poly-generation energy districts through a model based approach. Applied Thermal Engineering, 99 (2016) 291-301.
2. Ferrari M.L., Rivarolo M., Massardo A.F., 2016, Hydrogen production system from photovoltaic panels: experimental characterization and size optimization. Energy Conversion and Management, 116 (2016) 194-202.
3. Pietzcker RC, Stetter D, Manger S, Luderer G. Using the sun to decarbonize the power sector: the economic potential of photovoltaics and concentrating solar power. Applied Energy 2014; 135:704–20.
4. Arce P, Medrano M, Gil A, Oró E, Cabeza L. Overview of thermal energy storage (TES) potential energy savings and climate change mitigation in Spain and Europe. Applied Energy 2011; 88(8):2764–74.
5. Mahmood M., Traverso A., Traverso A. N., Massardo A.F., Marsano D., Cravero C., ―Thermal energy storage for CSP hybrid gas turbine systems: Dynamic modelling and experimental validation. Applied Energy Vol.212, 2018, pp: 1240–1251.
6. Ferrari M.L., Cuneo A., Pascenti M., Traverso A., Real-time state of charge estimation in thermal storage vessels applied to a smart polygeneration grid. Applied Energy, 206 (2017) 90-100.
7. Cuneo A., Ferrari M.L., Pascenti M., Traverso A., State of charge estimation of thermal storages for distributed generation systems. Energy Procedia, 61 (2014) 254-257.

8. Xu, B., Li, P., and Chan, C., 2015. Application of phase change materials for thermal energy storage in concentrated solar thermal power plants: A review to recent developments. Applied Energy 160, 286–307.
9. Fallahi, A., Guldentops, G., Tao, M., Granados-Focil, S., Dessel, S.V. 2017. "Review on solid-solid phase change materials for thermal energy storage: Molecular structure and thermal properties". Applied Thermal Engineering 127:1427-1441.
10. Zalba, B., Marín, J.M., Cabeza, L.F., Mehling, H. 2003. "Review on thermal energy storage with phase change: materials, heat transfer analysis and applications". Applied Thermal Engineering. Vol: 23 (3) 251-283.
11. S. Tescaria, G. Lantin, M. Lange, S. Breuer, C. Agrafiotis, M. Roeb, C. Sattler. 2015. "Numerical model to design a thermochemical storage system for solar power plant". Energy Procedia 75 (2015) 2137 – 2143.
12. Cot-gores, J., Castell, A., and Cabeza, L. F., 2012. "Thermochemical energy storage and conversion : A-state-of-the-art review of the experimental research under practical conditions". Renew. Sustain. Energy Rev. 16 5207–24.
13. S. Tescari, C. Agrafiotis, S. Breuer, L. de Oliveira, M. Neises-von Puttkamer, M. Roeb, C. Sattler. 2014, Thermochemical solar energy storage via redox oxides: materials and reactor/heat exchanger concepts. Energy Procedia 49 (2014)1034 – 1043.
14. Ganesh Balasubramanian, Mehdi Ghommem, Muhammad R. Hajj, William P. Wong, Jennifer A. Tomlin, Ishwar K. Puri. 2010. Modeling of thermochemical energy storage by salt hydrates. International Journal of Heat and Mass Transfer, 53 (2010) 5700–5706.
15. Mehdi Ghommem, Ganesh Balasubramanian, Muhammad R. Hajj, William P. Wong, Jennifer A. Tomlin, Ishwar K. Puri. 2011. Release of stored thermochemical energy from dehydrated salts. International Journal of Heat and Mass Transfer, 54 (2011) 4856–4863.
16. Armand Fopah Lele, Frédéric Kuznik, Holger U. Rammelberg, Thomas Schmidt Wolfgang K.L. Ruck. 2015. Thermal decomposition kinetic of salt hydrates for heat storage systems. Applied Energy 154 (2015) 447–458.
17. S. Tescari, C. Agrafiotis, S. Breuer, L. de Oliveira, M. Neises-von Puttkamer, M. Roeb, C. Sattler. 2014, Thermochemical solar energy storage via redox oxides: materials and reactor/heat exchanger concepts. Energy Procedia 49 (2014) 1034 – 1043.
18. Abhishek Singh, Stefania Tescari, Gunnar Lantin, Christos Agrafiotis, Martin Roeb, Christian Sattler. 2017, Solar thermochemical heat storage via the Co_3O_4/CoO looping cycle: Storage reactor modelling and experimental validation. Solar Energy 144 (2017) 453–465.
19. G. Karagiannakis, C. Pagkoura, A.G. Konstandopoulos, S. Tescari, A. Singh, M. Roeb, M. Lange, J. Marcher, A. Jové, C. Prieto, M. Rattenbury, A. Chasiotis, Thermochemical storage for CSP via redox structured reactors/heat exchangers: The RESTRUCTURE project, AIP Conference Proceedings, 1850(2017).
20. C. Pagkoura, G. Karagiannakis, E. Halevas, A.G. Konstandopoulos, Co3O4-based honeycombs as compact redox reactors/heat exchangers for thermochemical storage in the next generation CSP plants, AIP Conference Proceedings, 1734(2016).
21. Hutchings, K.N., Wilson, M., Larsen, P.A., Cutler, R.A., 2006. Kinetic and thermodynamic considerations for oxygen absorption/desorption using cobalt oxide. Solid State Ionics 177, 45–51.

22. Agrafiotis, C., Roeb, M., Sattler, C., 2016. Exploitation of thermochemical cycles based on solid oxide redox systems for thermochemical storage of solar heat. Part 4: Screening of oxides for use in cascaded thermochemical storage concepts. Solar Energy 139, 695–710.
23. S. Tescari , A. Singh, C. Agrafiotis, L. de Oliveira, S. Breuer, B. Schlögl-Knothe, M. Roeb, C. Sattler, 2017. Experimental evaluation of a pilot-scale thermochemical storage system for a concentrated solar power plant. Applied Energy 189 (2017) 66–75.
24. Schwarzboezl P, Pomp S, Koll G, Hennecke K, Hartz T, Schmitz M, et al. The solar tower in Jülich – first operational experiences and test results. SolarPACES, Perpignan, France; 2010.
25. Neises, M. Tescari, S. de Oliveira, L. Roeb, M. Sattler, C. Wong, B., Solar-heated rotary kiln for thermochemical energy storage. Solar Energy 2012, 86, (10), 3040-3048.
26. T. Nagel, H. Shao, A.K. Singh, N. Watanabe, C. Roßkopf, M. Linder, A. Wörner, O. Kolditz. Non-equilibrium thermochemical heat storage in porous media: Part 1-Conceptual model. Energy 60 (2013) 254-270.
27. Zhongyang Luo, Cheng Wang, Gang Xiao, Mingjiang Ni, Kefa Cen. 2014. Simulation and experimental study on honeycomb-ceramic thermal energy storage for solar thermal systems. Applied Thermal Engineering 73 (2014) 620-626.
28. Guangwei Yang, Gang Xiao, Tianfeng Yang, Mingjiang Ni, Kefa Cen. 2017. Thermal Kinetics of CuO/Cu2O redox system. SolarPaces 2017.
29. A.F. Mills, Heat Transfer, Second Edition, Prentice-Hall, New Jersey, 1999.
30. Pagkoura, C., Karagiannakis, G., Zygogianni, A., Lorentzou, S., Kostoglou, M., Konstandopoulos, G.A., Rattenburry, M., Woodhead, W.J., 2014. Cobalt oxide based structured bodies as redox thermochemical heat storage medium for future CSP plants. Sol. Energy 108, 146–163.
31. Feng Hongyan, Study on Heat Transfer Enhancement about the Regenerator of Regenerative Heat Exchanger, South China University of Technology, 2012, pp.77.